Synthesis of delafossite-derived phases, $R\mathrm{CuO}_{2+\delta}$ with $R=$ Y, La, Pr, Nd, Sm, and Eu, and observation of spin-gap-like behavior

Kazuyuki Isawa,* Yuji Yaegashi, Motoharu Komatsu, Mitsugu Nagano, and Shiroshi Sudo
Research and Development Center, Tohoku Electric Power Company, Incorporated, 2-1 Nakayama 7-chome, Aoba-ku, Sendai 981, Japan

Maarit Karppinen and Hisao Yamauchi
Materials and Structures Laboratory, Tokyo Institute of Technology, Nagatsuta, Midori-ku, Yokohama 226, Japan
(Received 5 February 1997)

The structural and physical properties of layered cuprates of a $R\mathrm{CuO}_2$ delafossite structure have been investigated for various rare-earth elements R: Y, La, Pr, Nd, Sm, and Eu. An oxygen-rich delafossite-derived phase, $R\mathrm{CuO}_{2+\delta}$ ($\delta \geqslant 0.5$), as previously reported by Cava *et al.* for $R=$ Y and La was found for all the other R presently studied. Each as-sintered $R\mathrm{CuO}_2$ sample appeared to have a nearly stoichiometric oxygen content, but by thermal oxidation excess oxygen atoms corresponding to $\delta \geqslant 0.5$ per formula unit could be loaded into the lattices. Although electrical resistivity (ρ) of the oxygen-rich $R\mathrm{CuO}_{2+\delta}$ samples exhibited semiconducting behavior at temperatures below 325 K a couple of samples showed anomalous temperature dependences in ρ at low temperatures. Unusual temperature dependence of magnetic susceptibility (χ), was observed for Ca-doped $\mathrm{YCuO}_{2+\delta}$ samples, but not for the other $R\mathrm{CuO}_{2+\delta}$ phases. If the Curie term was subtracted from the susceptibility of (Y,Ca)$\mathrm{CuO}_{2+\delta}$, the remaining part of χ decreased monotonically with decreasing temperature down to $\sim$100 K, and then leveled off with a finite value. Assuming that this finite value could be attributed to the Pauli paramagnetism of free carriers, the χ vs T characteristics were compared with those of other layered cuprates, such as $\mathrm{SrCu}_2\mathrm{O}_3$, $(\mathrm{Sr,Ca})_{14}\mathrm{Cu}_{24}\mathrm{O}_{41}$, and (La,Sr)$\mathrm{CuO}_{2.5}$, which have been reported to exhibit spin-gap behavior. [S0163-1829(97)08030-2]

I. INTRODUCTION

Because of low dimensionality, layered cuprates (other than known high-T_c superconductors) have attracted the attention of researchers in the field of new materials with novel quantum functions. Intense studies have been done on two-dimensional (2D) ladder compounds[1–7] such as $\mathrm{Sr}_{n-1}\mathrm{Cu}_{n+1}\mathrm{O}_{2n}$ ($n=3,7,11,\ldots$) and $\mathrm{LaCuO}_{2.5}$ in order to verify the theoretical predictions[8] concerning a spin-gap and d-wave superconductivity in lightly hole-doped compounds with even-number legs. Recently, superconductivity was confirmed for a two-leg ladder system of $(\mathrm{Sr,Ca})_{14}\mathrm{Cu}_{24}\mathrm{O}_{41}$ under a high pressure of $\sim$3 GPa.[9] But T_c ($\sim$10 K) was significantly lower than that previously predicted.[8] Another interesting quantum phenomenon has been reported for one-dimensional (1D) Cu-O chain materials of $\mathrm{Sr}_2\mathrm{CuO}_3$ and related phases, e.g., $\mathrm{Ca}_2\mathrm{CuO}_3$ and SrCuO_2.[10–12] Motoyama, Eisaki, and Uchida[11] demonstrated that the magnetic susceptibility of $\mathrm{Sr}_2\mathrm{CuO}_3$ was consistent with theoretical calculations for an $s=1/2$ 1D Heisenberg antiferromagnetic system.

$R\mathrm{CuO}_2$ delafossites have acquired a position of layered cuprates of interest, as well.[13,14] However, to our knowledge, the physical properties of the delafossites have not been extensively characterized, probably due to difficulties in the sample preparation. Various transition-metal oxides are known to have structures of delafossite (CuFeO_2) type. The delafossite is generally expressed as $A^+B^{3+}\mathrm{O}_2$. The stacking sequence of the linearly coordinated A^+-O block and the six-coordinated B^{3+}-O block along the **c** direction is different depending on the material. As a consequence, a variety of polytypes are formed. In the ternary R-Cu-O phase diagram, the $R\mathrm{CuO}_2$ delafossite structure has been found for the following rare-earth elements (R): Y, La, Pr, Nd, Sm, and Eu.[13,14] Schematic illustrations of the crystal structures of the $3R$ and $2H$ polytypes are shown in Figs. 1(a) and 1(b).[15,16] It should be note that the characteristic 2D triangular copper layers are stacked along the **c** direction in both structures. The $3R$ polytypes of $R\mathrm{CuO}_2$ delafossites in which three elementary double layers per unit cell ($Z=3$) are stacked

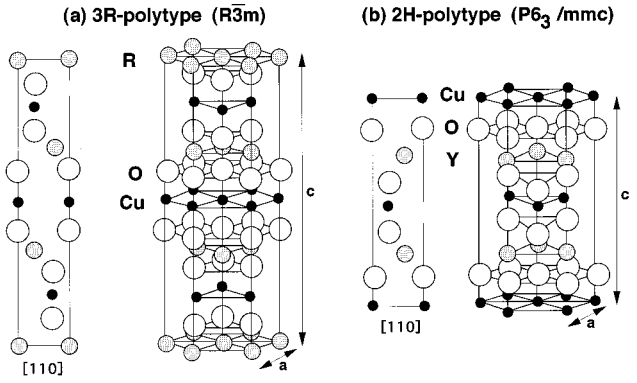

FIG. 1. Schematic representation of crystallographic structure of delafossites (Refs. 15, 16): (a) $3R$ polytype and (b) $2H$ polytype. A view of the structure in the [110] plane is also shown. The shaded, closed, and open circles indicate R, Cu, O atoms, respectively. In the basal plane, Cu atoms sit in the two-dimensional triangular plane lattices. The Cu^+ ions are linearly coordinated with oxygen, and R^{3+} ions are six-coordinated with oxygen.

along the **c** direction have been reported since 1960's for all the rare-earth elements studied.[13] The unit cell is rhombohedral with the $R3m$ symmetry. On the other hand, the $2H$ polytype which has been obtained only for $R=$Y belongs to hexagonal with space group $P6_3/mmc$.[14]

It has been anticipated that such a 2D triangular plane lattice would display unusual magnetic behavior due to a geometrical antiferromagnetic frustration. In accordance with the prediction, several groups have reported interesting magnetic properties for delafossite-type vanadates.[17,18] Furthermore, Cava *et al.*[19] reported that new delafossite-derived oxygen-rich $RCuO_{2+\delta}$ phases were obtained by thermal oxidation for $YCuO_2$, (Y,Ca)CuO_2, and $LaCuO_2$. The oxidized samples became more conductive with increasing δ. This indicates that mobile carriers are doped into the structure through the loading oxygen. However, except for those with $R=$Y and La, neither physical properties nor carrier doping effects have been reported yet. In addition, the carrier doping studies in the 2D triangular lattices are supposed to yield interesting results in comparison with other low-dimensional systems, such as the CuO_2 planes (in the high-T_c superconducting cuprates), the Cu_2O_3 ladder compounds, and other cuprates having the Cu^{2+} ($3d^9$) configuration with $s=1/2$. Therefore, it is worth to clarify the physical properties of doped $RCuO_{2+\delta}$ phases in terms of various rare-earth ions. In this work, we synthesized polycrystalline $RCuO_2$ samples and studied the oxidation processes, resulting in formal copper valences even higher than +II. The electrical and magnetic properties of the synthesized materials were also investigated. The peculiar magnetic properties found especially in Ca-doped $YCuO_{2+\delta}$ samples, were interpreted using a model proposed for Heisenberg ladder compounds.

II. EXPERIMENT

Except for $R=$Y, polycrystalline samples of $RCuO_2$ delafossites were prepared by a solid-state reaction technique from reagent grade R_2O_3 and Cu_2O powders. The powder mixtures were pressed into pellets and fired at 900–1075 °C for 12–24 h in a vacuum furnace with molybdenum heater in order to prevent the oxidation of monovalent copper. A typical background vacuum pressure inside the furnace was $\sim 4\times10^{-6}$ Torr at high temperatures. Synthesis of $YCuO_2$, on the other hand, was found to be considerably more difficult. Ca doping was found effective to stabilize the $YCuO_2$ phase by means of the following procedure. Intermediate reactants[20] with the nominal composition of $(Y_{1-x}Ca_x)_2Cu_2O_5$ ($0\leqslant x\leqslant 0.15$) were synthesized from reagent-grade Y_2O_3, $CaCO_3$, and CuO powders by firing in air at 950–1000 °C for 80 h. After grinding, the calcined $(Y,Ca)_2Cu_2O_5$ powders were pressed into pellets and sintered at 1150–1175 °C for 16 h in N_2/60–100 ppm O_2 gas mixtures, with a slow cooling (−2 °C/min) down to room temperature.

The phase content and the lattice parameters were determined by powder x-ray-diffraction (XRD) analysis using Cu $K\alpha$ radiation (Rigaku RINT-2500 HF). Oxidation characteristic of as-sintered samples was studied up to 1000 °C using a commercial thermogravimetric apparatus (TA Instruments TGA-2950). The sample weight was about 30 mg and the heating rate was 1 °C/min. Oxygen contents in the as-sintered and oxidized samples were analyzed by the following two methods: (i) thermogravimetric hydrogen reduction (H_2/TG) measurements and (ii) Cu(+I)/Cu(+II) coulometric titrations. Details of the methods have been reviewed elsewhere.[21] Electrical resistivity of the samples was measured by a conventional dc four-probe method. The dc magnetic susceptibility was measured using a superconducting quantum interference device magnetometer.

III. RESULTS AND DISCUSSION

A. Synthesis of $RCuO_2$ and Ca-doped $YCuO_2$ delafossites

Figure 2(a) shows powder XRD patterns for the synthesized $RCuO_2$ samples. Although very small peaks from unreacted R_2O_3 and Cu_2O were still detected, nearly all the diffraction peaks were able to be assigned to the rhombohedral unit cell of the $3R$ polytype. The corresponding optimized sintering conditions are summarized in Table I. Except in the case of $R=$Nd, the samples were synthesized at temperatures $\geqslant$1000 °C in a high vacuum of $\sim 4\times10^{-6}$ Torr. Note that, however, Zr-foil wrapping was necessary to obtain the $PrCuO_2$ phase. For $NdCuO_2$, the optimum sintering temperature was found to be around ~900 °C; sintering at temperatures higher than 900 °C resulted in the decomposition of the $NdCuO_2$ phase into Nd_2O_3, Cu_2O, and Cu metal.

In Fig. 2(b), the lattice parameters **a** and **c** are represented with respect to the rare-earth ionic radius r_R. The value of **a** decreases pseudolinearly as a function of r_R descending from La^{3+} ($r_R=1.032$ Å) to Eu^{3+} ($r_R=0.947$ Å).[22] This tendency is in good agreement with the previous data reported in Ref. 13. On the other hand, the **c** value is nearly independent of r_R.

Powder XRD patterns for the $(Y_{1-x}Ca_x)CuO_2$ ($0\leqslant \mathbf{x} \leqslant 0.15$) samples are shown in Fig. 3(a). For the samples with $0<\mathbf{x}\leqslant 0.1$, almost all the diffraction peaks could be assigned to a hexagonal unit cell of the $2H$ polytype, and the lattice parameters were determined to be **a**~3.52 Å and **c** ~11.42 Å. Thus, the samples with $0<\mathbf{x}\leqslant 0.1$ are considered to be nearly single phase. Some unidentified diffraction peaks were detected for the samples with $\mathbf{x}\geqslant 0.15$. The diffraction pattern for the sample with $\mathbf{x}=0$, on the other hand, included peaks due to the $3R$ polytype[23] besides those of the $2H$ polytype. Furthermore, the peak due to the 102 reflection was rather broad for the $\mathbf{x}=0$ sample, but gradually sharpened as **x** increased. Such broad peaks are generally caused by stacking faults as described in Refs. 14 and 19. The difficulties in isolating the $3R$ and $2H$ polytypes of $YCuO_2$ are probably due to a very small difference in the thermodynamical free energies between these two phases.

Figure 3(b) shows the lattice parameters, **a** and **c**, with respect to Ca content, **x** in $(Y_{1-x}Ca_x)CuO_2$. The value of **a** first decreases quasilinearly as **x** increases up to 0.1 and then saturates to a constant value. Conversely, the value of **c** increases quasilinearly with increasing **x** for the samples with $\mathbf{x}\leqslant 0.15$. These results indicate that Ca ions substitute the Y site in the range of $0<\mathbf{x}\leqslant 0.1$. Both of the lattice parameters are rather similar to those reported in the literature for the $2H$ polytype.[14,19] The slight discrepancy between the present results and those reported previously is likely due to the difference in the oxygen content in the samples.

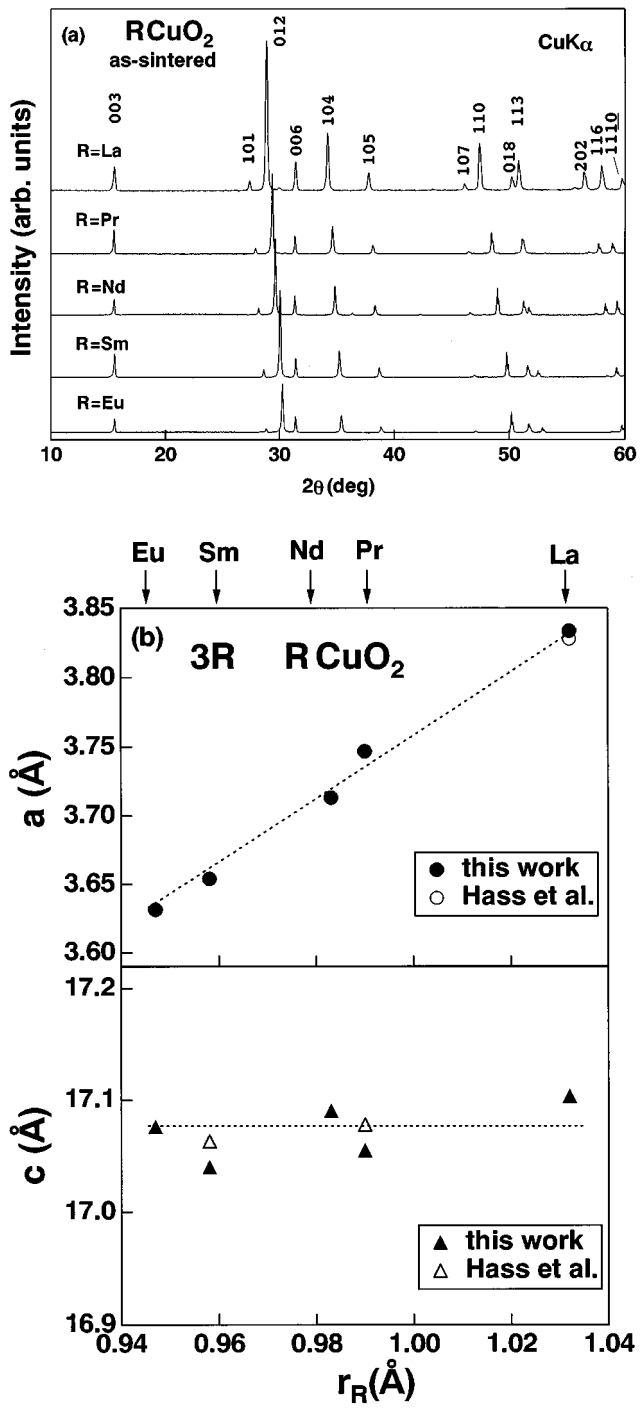

FIG. 2. (a) Powder XRD patterns for $R\mathrm{CuO_2}$ with various rare-earth elements (R=La, Pr, Nd, Sm, and Eu). Almost all diffraction peaks are assigned with a rhombohedral unit cell of the $3R$ polytype. (b) Lattice constants **a** and **c** as a function of rare-earth ionic radius r_R.

B. Oxidation of $R\mathrm{CuO_2}$ and Ca-doped $\mathrm{YCuO_2}$ delafossites

A typical oxidation TG curve, obtained for a $\mathrm{NdCuO_2}$ sample under an $\mathrm{O_2}$ atmosphere is shown in Fig. 4. Upon heating at 1 °C/min, the weight is unchanged at temperatures below 200 °C. The most significant weight gain starts at ~370 °C. On continuously heating, the sample weight reaches a plateau between 370 and 600 °C, and then decreases rapidly above 600 °C before the final decomposition into $\mathrm{Nd_2CuO_4}$ and CuO. The recorded powder XRD pattern indicates that the oxidized $\mathrm{NdCuO_{2+\delta}}$ sample (at ~370 °C) contain the same delafossite-derived phase which has been previously reported for $\mathrm{LaCuO_{2+\delta}}$.[19] For all the as-sintered $R\mathrm{CuO_2}$ and $(\mathrm{Y_{1-x}Ca_x})\mathrm{CuO_2}$ samples, careful TG measurements were performed, and essentially similar results were obtained. However, in order to isolate the oxygen-rich phases prolonged post-annealing periods, usually for 1–4 days, were required. The post-annealing conditions used for the $R\mathrm{CuO_2}$ and $(\mathrm{Y_{1-x}Ca_x})\mathrm{CuO_2}$ samples are summarized in Table II.

TABLE I. Sintering conditions for $R\mathrm{CuO_2}$ in vacuum furnace.

	Sintering conditions	Vacuum pressure (PO_2)
$\mathrm{LaCuO_2}$	1000 °C, 12 h	4×10^{-6} Torr
$\mathrm{PrCuO_2}$	1000 °C, 24 h (Zr foil)	4×10^{-6} Torr
$\mathrm{NdCuO_2}$	900 °C, 12 h (×2)	4×10^{-6} Torr
$\mathrm{SmCuO_2}$	1075 °C, 24 h	3.5×10^{-6} Torr
$\mathrm{EuCuO_2}$	1050 °C, 24 h	3.5×10^{-6} Torr

Figure 5(a) shows the powder XRD patterns of the oxidized $R\mathrm{CuO_{2+\delta}}$ samples which are totally different from those obtained for the as-sintered samples [Fig. 2(a)]. Although some broad unidentified peaks were detected, major diffraction peaks could be indexed according to the hexagonal supercell of the $2H$ polytype. The lattice parameters for the oxidized $R\mathrm{CuO_{2+\delta}}$ samples as a function of the rare-earth ionic radius r_R are shown in Fig. 5(b). The supercell parameters are estimated to be $\mathbf{a}\approx\sqrt{3}a_0$ (~6.42 Å) and $\mathbf{c}\leqslant 2/3c_0$(~10.5 Å), where a_0 and c_0 are the lattice parameters obtained for the $3R$-polytype $R\mathrm{CuO_2}$ delafossites.

Powder XRD patterns of the $(\mathrm{Y_{1-x}Ca_x})\mathrm{CuO_{2+\delta}}$ samples after post-annealing in flowing $\mathrm{O_2}$ gas are shown in Fig. 6(a). For all the patterns with $x\leqslant 0.1$, the major phase was identified to be an orthorhombic supercell with $\mathbf{a}\approx\sqrt{3}a_0'$ (~6.18 Å), $\mathbf{b}\approx 2a_0'$ (~7.14 Å), and $\mathbf{c}\approx c_0'$(~11.2 Å), as previously reported for $\mathrm{YCuO_{2.55}}$.[19] Besides those for the oxygen-rich phase, unidentified small diffraction peaks were detected, especially for the samples with $\mathbf{x}=0$ and $\mathbf{x}=0.075$, as marked with solid circles (●). Figure 6(b) shows the lattice parameters versus Ca content **x** for the oxidized $(\mathrm{Y_{1-x}Ca_x})\mathrm{CuO_{2+\delta}}$ samples. For all these samples, both **a** and **b** increase gradually against the Ca content **x**, while **c** is nearly independent of **x**.

C. Analyses of the oxygen content before and after the oxidation

Oxygen content of the as-sintered samples was determined by the thermogravimetric reduction method, which has commonly been adopted for high-T_c copper-oxide superconductors.[21] In this method, the sample is heated up to 1000 °C in flowing 96.4% Ar-3.6% $\mathrm{H_2}$ in a thermobalance, and from the total weight loss the amount of oxygen in the starting material can be calculated if the final products are known. Since the as-sintered $R\mathrm{CuO_2}$ samples easily absorb humidity fresh powdered samples were prepared before the measurements. In Fig. 7, a typical TG curve obtained for the as-sintered $\mathrm{NdCuO_y}$ sample under a reducing atmosphere is

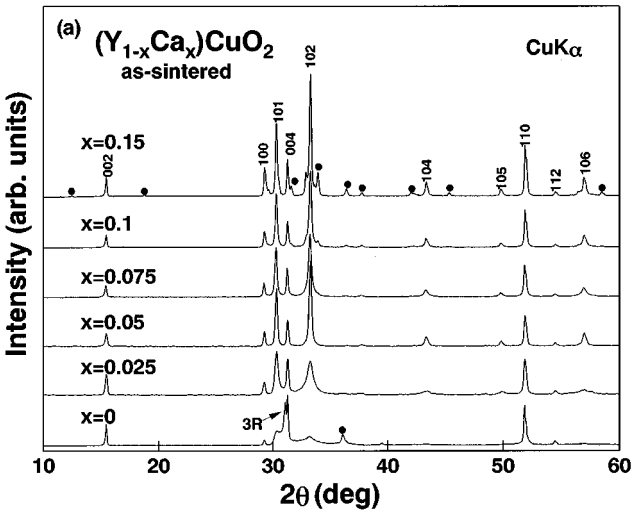

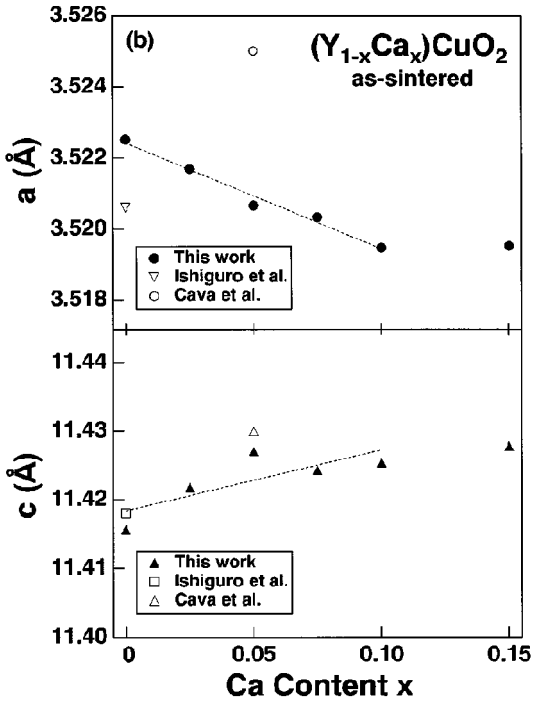

FIG. 3. (a) Powder XRD patterns for $(Y_{1-x}Ca_x)CuO_2$ with $0 \leqslant \mathbf{x} \leqslant 0.15$. For the samples with $0 < \mathbf{x} \leqslant 0.1$, almost all diffraction peaks are indexable with the lattice parameters **a** ~ 3.52 Å and **c** ~ 11.42 Å. Unidentified peaks are marked with solid circles. (b) Lattice constant, **a** and **c** as a function of Ca content, **x**: (●, ▲), this work; (▽, □), Ishiguro *et al.* (Ref. 14); (○, △), Cava *et al.* (Ref. 19). In the present results, the $(Y_{1-x}Ca_x)CuO_{2+\delta}$ samples with $0 < \mathbf{x} \leqslant 0.1$ are nearly single phase.

shown. When heating at 2 °C/min, the sample was rather stable at temperatures below ~200 °C. The reduction occurred in two steps above 200 °C. The reduction products were confirmed by XRD to be Nd_2O_3 and Cu metal. Furthermore, the oxygen content of the oxidized samples was observed *in situ* on annealing the as-sintered samples in a thermobalance as shown in Fig. 4, since the amount of oxygen in the starting materials was already fixed. For all the samples, careful TG measurements under reducing and oxidizing atmospheres were carried out, and the obtained oxygen contents in the as-sintered and post-annealed samples are summarized in Table III. In this table, the results of the additional Coulometric titration analyses are shown in brackets. The accuracy of the oxygen content determination by the TG methods corresponds to an error of ±0.03 oxygen atoms per formula unit (f.u.). In the case of the Coulometric titrations the error is supposed to be ±0.02. Each as-sintered sample appeared to have a nearly stoichiometric oxygen content, namely, 2.00±0.03 oxygen atoms per f.u. Upon annealing under oxidizing conditions excess oxygen corresponding to ⩾0.5 atoms per f.u. was found to incorporate into the structures for all the samples studied. Thus, in the case of R=La, for example, formal values of the copper valence in the as-sintered and post-annealed samples are +1.04 and +2.28, respectively.

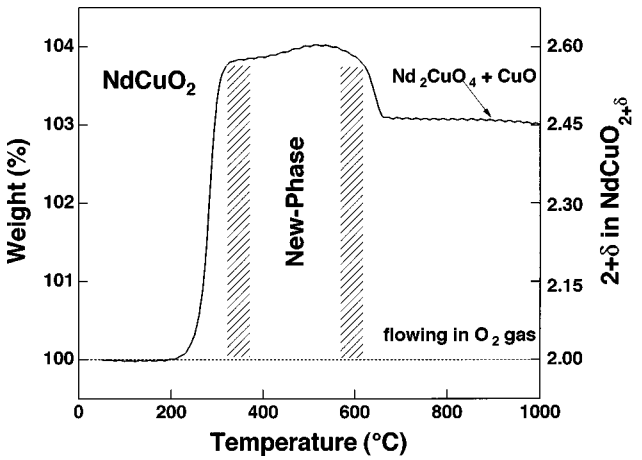

FIG. 4. Change in weight of powdered $NdCuO_2$ sample in a commercial TG on heating in flowing O_2 gas at 1 °C/min to 1000 °C. The delafossite-type $NdCuO_2$ phase remains below ~200 °C, and then, significant weight gain begins at higher temperatures. Oxygen content $2+\delta$, corresponding to weight gain is shown in the right-hand scale.

D. Electrical properties

Figure 8(a) shows the temperature dependence of electrical resistivity (ρ) in a logarithmic scale for the oxidized $R CuO_{2+\delta}$ and $(Y,Ca)CuO_{2+\delta}$ samples. The magnitude of ρ around room temperature for all the $R CuO_2$ samples without excess oxygen ($\delta=0$) is as high as $\geqslant 10^5$ Ω cm. The ρ vs T curves for all the samples except for $PrCuO_{2.62}$ are quite similar. That is, for each sample, the ρ vs T curve shows

TABLE II. Post-annealing conditions for bar-shaped $R CuO_2$ and Ca-doped $YCuO_2$ in flowing O_2 gas.

	Annealing conditions
$LaCuO_2$	380 °C, 96 h
$PrCuO_2$	400 °C, 96 h
$NdCuO_2$	370 °C, 96 h
$SmCuO_2$	400 °C, 96 h
$EuCuO_2$	400 °C, 96 h
$YCuO_2$	450 °C, 96 h
$Y_{0.95}Ca_{0.05}CuO_2$	450 °C, 96 h
$Y_{0.9}Ca_{0.1}CuO_2$	450 °C, 96 h

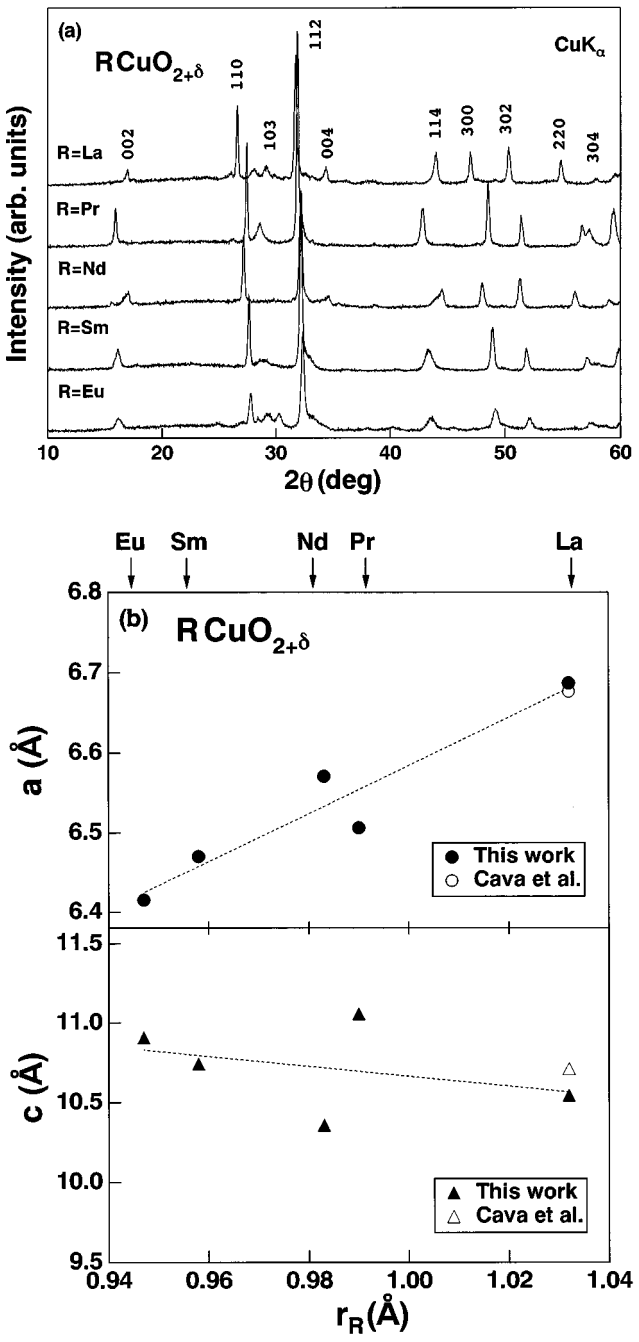

FIG. 5. (a) Powder XRD patterns for oxidized $R\mathrm{CuO}_{2+\delta}$ with various rare-earth elements (R=La, Pr, Nd, Sm, and Eu). Post-annealing conditions in O_2 are summarized in Table II. Almost all diffraction peaks are assigned with hexagonal supercell parameters of $\mathbf{a}\approx\sqrt{3}a_0(\sim 6.42$ Å) and $\mathbf{c}\leqslant 2/3c_0(\sim 10.5$ Å). (b) Lattice constants **a** and **c** as a function of rare-earth ionic radius r_R: (●, ▲), this work; (○, △), Cava *et al.* for $\mathrm{LaCuO}_{2+\delta}$ (Ref. 19).

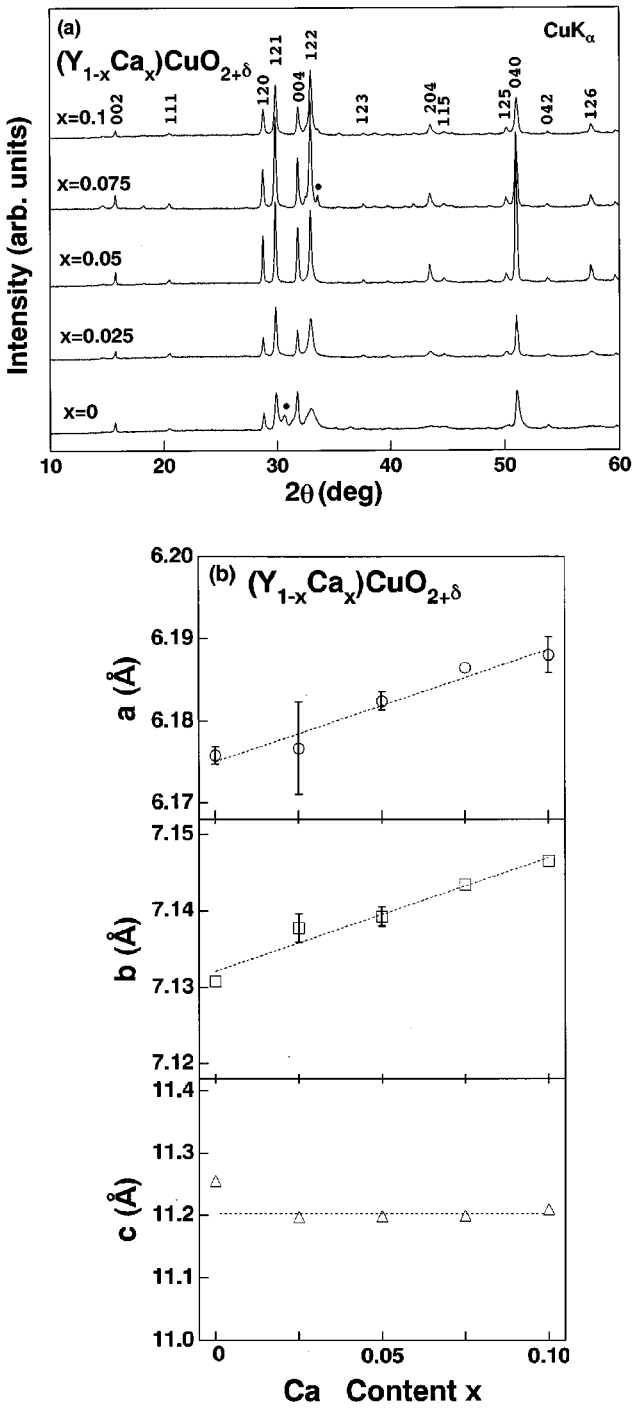

FIG. 6. (a) Powder XRD patterns for $(\mathrm{Y}_{1-x}\mathrm{Ca}_x)\mathrm{CuO}_{2+\delta}$ with $0\leqslant\mathbf{x}\leqslant 0.1$ after post annealing in flowing O_2 gas. Each sample has an orthorhombic distortion of supercell parameters with $\mathbf{a}\approx\sqrt{3}a_0'$ (~ 6.18 Å), $\mathbf{b}\approx 2a_0'(\sim 7.14$ Å), and $\mathbf{c}\approx c_0'(\sim 11.2$ Å). Impurity peaks are marked with solid circles. (b) Lattice constants, **a**, **b**, and **c** as a function of Ca content **x**.

semiconducting behavior being in good agreement with the data previously reported for $\mathrm{YCuO}_{2+\delta}$ and $\mathrm{LaCuO}_{2+\delta}$.[19] For $\mathrm{PrCuO}_{2.62}$, ρ increases rather rapidly with decreasing temperature in comparison with the other samples, and turns into insulating behavior at temperatures below 150 K. In the $\mathrm{NdCuO}_{2.63}$, $\mathrm{SmCuO}_{2.62}$, and $\mathrm{EuCuO}_{2.65}$ samples, anomalous behavior is observed at low temperatures around 50 K. Since the electrical properties in $R\mathrm{CuO}_{2+\delta}$ samples are likely to be related to magnetic properties, these anomalies in the ρ vs T curves will be discussed later. In the case of the $(\mathrm{Y,Ca})\mathrm{CuO}_{2+\delta}$ system, on the other hand, the samples become more conductive with increasing Ca content. This is probably due to a slight enhancement in the mobile carrier density through the partial substitution of trivalent Y by divalent Ca. In Fig. 8(b), the resistivities ($\ln\rho$) as a function of reciprocal temperature ($\mathbf{T}^{-1}$) for the oxidized $R\mathrm{CuO}_{2+\delta}$ and $(\mathrm{Y,Ca})\mathrm{CuO}_{2+\delta}$ samples are replotted. The obtained $\ln\rho$ vs

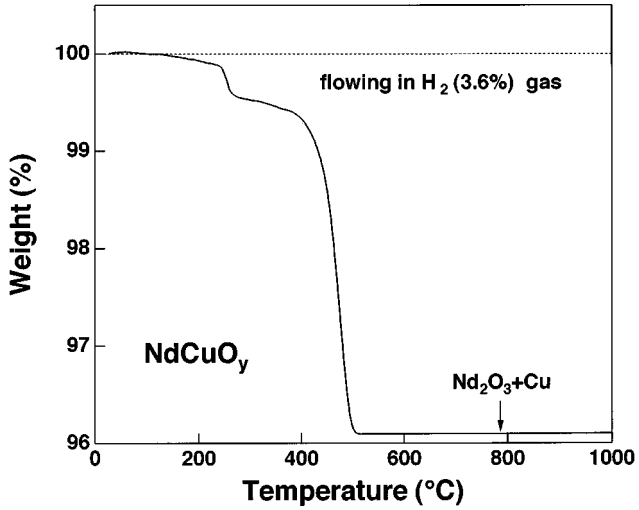

FIG. 7. Typical TG curve of $NdCuO_y$ in reducing atmosphere. By powder XRD measurements, the $NdCuO_y$ phase was found to be decomposed into Nd_2O_3 and Cu metal above $\geqslant 500$ °C. For each sample, oxygen content (y) in the sample is calculated by the following equation: $RCuO_y + H_2 \rightarrow R_2O_3 + Cu + H_2O(\uparrow)$.

$\mathbf{T}^{-1}$ curves are pseudolinear in the temperature range between 325 and 200 K with the exception of the $PrCuO_{2.62}$ case. Furthermore, the slope of the curves, i.e., $d(\ln \rho)/d(\mathbf{T}^{-1})$, is nearly independent of R. The activation energies (E_a) are obtained from the following Arrhenius equation:

$$\rho(T) = \rho_0 \exp(E_a/k_B T), \tag{1}$$

where ρ_0 is a temperature-independent constant and k_B is the Boltzmann constant. According to the Arrhenius plots shown in Fig. 8(b), the electrical conduction in $RCuO_{2+\delta}$ is likely due to thermally activated carriers. The obtained values of E_a were ~ 0.2 eV for all the samples other than for $R = \mathrm{Pr}$. Since pellets of the obtained samples are not quite dense, further studies are required to clinch whether the grain-boundary effects on resistivity are dominant or not.

Previously, high electrical conductivities of $\sim 10^6\ \Omega^{-1}\ \mathrm{cm}^{-1}$ have been reported for platinum and palladium delafossites.[24] In both of these structures (ABO_2) the noble-metal ions occupy the same site as copper in $RCuO_2$

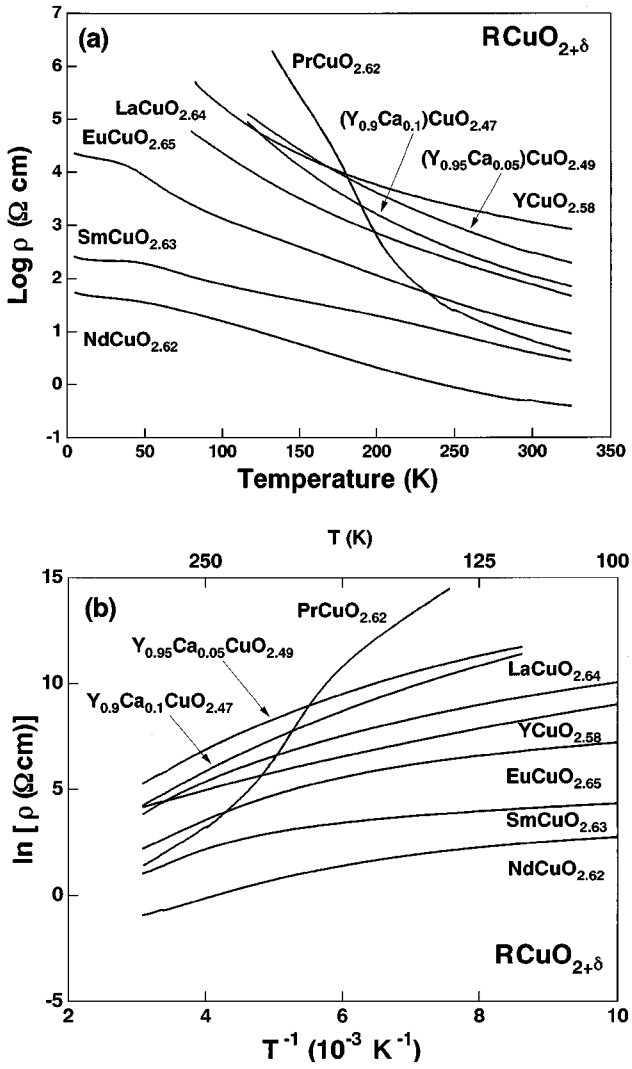

FIG. 8. (a) Temperature dependence of electrical resistivity (ρ) for oxidized $RCuO_{2+\delta}$ and $(Y_{1-x}Ca_x)CuO_{2+\delta}$ samples in logarithmic scale. Note that the sample with $x = 0$ included the minor impurity phase of $3R$-polytype $YCuO_2$ delafossite. (b) The relationship between $\ln \rho$ and $\mathbf{T}^{-1}$ for the oxidized samples.

TABLE III. Oxygen content, $2 + \delta$, in the $RCuO_{2+\delta}$ and Ca-doped $YCuO_{2+\delta}$ samples as analyzed by thermogravimetric (TG) measurements. In comparison, oxygen content obtained by the Coulometric titration is shown in the bracket.

	As-sintered	Post-annealed in flowing O_2 gas
$LaCuO_{2+\delta}$	2.02 (±0.03) $Cu^{+1.04}$	2.64 (±0.03) $Cu^{+2.28}$
	[2.03 (±0.02)]	[2.63 (±0.02)]
$PrCuO_{2+\delta}$	2.00 (±0.03)	2.62 (±0.03)
$NdCuO_{2+\delta}$	2.02 (±0.03)	2.62 (±0.03)
$SmCuO_{2+\delta}$	2.09 (±0.03)	2.63 (±0.03)
$EuCuO_{2+\delta}$	2.04 (±0.03)	2.65 (±0.03)
$YCuO_{2+\delta}$	2.08 (±0.03)	2.58 (±0.03)
$Y_{0.95}Ca_{0.05}CuO_{2+\delta}$	[2.02(±0.02)]	2.49 (±0.03)
$Y_{0.9}Ca_{0.1}CuO_{2+\delta}$	[1.99(±0.02)]	2.47 (±0.03)

(A site), and the conduction band is supposed to be caused by strong metal-metal interactions among the A-site ions due to the rather short metal to metal distances (d_M), e.g., $d_M \sim 2.83$ Å for Pt-Pt in $PtCoO_2$. Contrary to such a short d_M in the noble compounds, much larger d_M for Cu-Cu is observed for the RCuO$_2$ phases, e.g., $d_M \sim 3.83$ Å in $LaCuO_2$. For RCuO$_2$, d_M slightly depends on r_R which affects the **a**-axis length. Therefore, the conduction mechanisms in RCuO$_2$ phases and oxidized phases ($\delta \geqslant 0.5$) are likely different according to the aforementioned model which typically describes the conduction in Ti_2O_3 of a corundum structure.[25] Based on photoabsorption spectra, on the other hand, Cava *et al.*[19] concluded that the conduction holes in both $YCuO_{2+\delta}$ and $LaCuO_{2+\delta}$ had Cu $3d$ character, but the overlap between O $2p$ and Cu $3d$ was small, as compared with that in high-T_c superconducting cuprates, causing the high resistivities of these compounds. Band-structural analyses of RCuO$_{2+\delta}$, especially in the vicinity of the Fermi level, would be of interest for future studies.

E. Magnetic properties

Figure 9(a) shows the temperature dependence of the dc magnetic susceptibility (χ) for the oxygen-rich RCuO$_{2+\delta}$ samples. Furthermore, for the samples with R = Pr, Nd, and Eu, the reciprocal susceptibilities χ^{-1} as a function of temperature are replotted in Fig. 9(b). Now, we discuss the effect of post-annealing on χ for the case of R = Sm, for example. In comparison with oxidized $SmCuO_{2.63}$, χ of as-sintered $SmCuO_{2.09}$ (dashed line) is nearly independent of temperature above 10 K, and below 10 K it slightly increases with decreasing temperature. The former behavior is consistent with that expected for a nonmagnetic system ($3d^{10}$ for Cu^+ ions), while the latter is supposed to be due to small magnetic impurities which are not detected by XRD analysis and/or lattice imperfections. It was also found that temperature-independent susceptibility χ_0 increases slightly upon post-annealing. The slight increase in χ_0 can be attributed to the Pauli paramagnetism of free carriers, since the oxidized sample is conductive, though not a metallic conductor but a semiconductor. Similar results in terms of χ_0 were observed for all the oxidized RCuO$_{2+\delta}$ samples.

On the other hand, the temperature dependence of χ in all the oxidized RCuO$_{2+\delta}$ samples exhibited a basically Curie-Weiss-type behavior. For each sample, χ monotonically increased on cooling down to 2 K. As clearly seen in Fig. 9(b), all the χ^{-1} vs T curves are essentially straight at temperatures above $\geqslant 100$ K. For each sample, an effective magnetic moment μ_{eff} was estimated by the curve fitting based on the Curie-Weiss relation:

$$\chi = \chi_0 + \frac{C}{(T-\theta)}, \tag{2}$$

where C is the Curie constant and θ is the asymptotic Curie temperature. Now, we can calculate μ_{eff} for each sample using

$$C = \frac{N_m \mu_{\text{eff}}^2}{3k_B}, \tag{3}$$

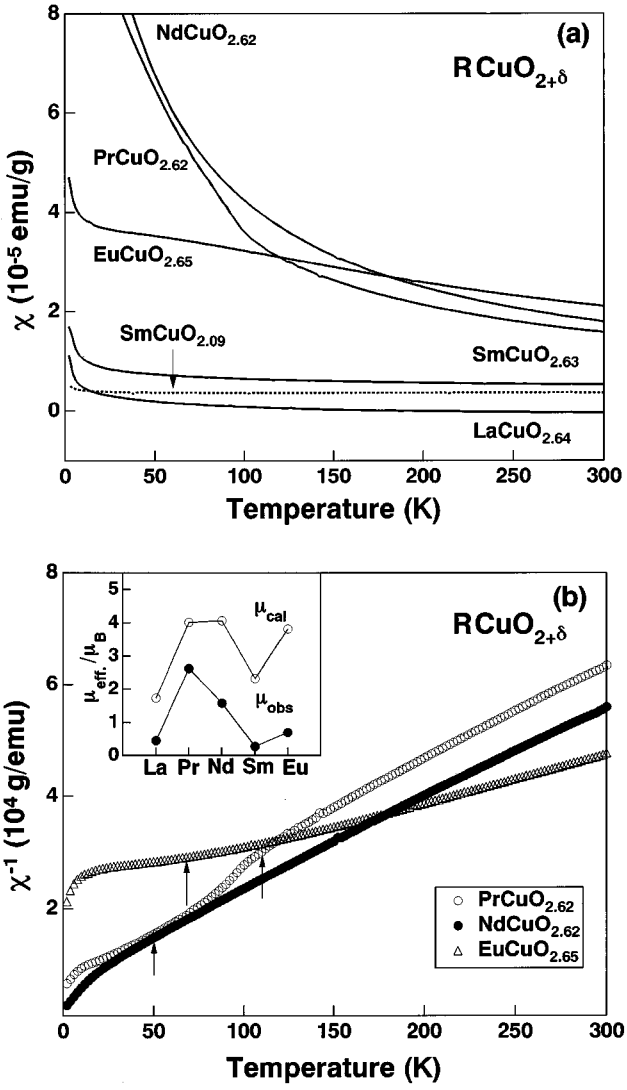

FIG. 9. (a) Temperature dependence of the magnetic susceptibility (χ) for oxygen-rich RCuO$_{2+\delta}$ samples. To comparison, χ vs T curve for as-sintered $SmCuO_{2.09}$ is also plotted (dashed line). (b) The reciprocal susceptibility $[1/(\chi-\chi_0)]$ as a function of temperature for the sample with R = Pr, Nd, and Eu. Arrow indicates the temperature deviated from the straight line. Inset: the effective magnetic moment μ_{eff} with respect to rare-earth elements. The calculated values μ_{cal} using the table in the literature (Ref. 26) is shown in the open circle. The obtained values μ_{obs} based upon the Curie-Weiss relation [Eq. (2)] is plotted as a solid circle.

where N_m is the number density of magnetic ions, i.e., R and/or Cu per unit volume. The μ_{eff} values are shown in the inset of Fig. 9(b) (solid circles), being calculated from the linear portion of the $(\chi-\chi_0)^{-1}$ vs T plot. Assuming that R and Cu ions are, respectively, trivalent and divalent, the average magnetic moment μ_{cal} is also plotted for each sample in the inset (open circles). In this calculation, we employed values for the effective magnetic moments of R^{3+} and Cu^{2+} ions tabulated in Ref. 26. A typical value obtained by the Curie-Weiss fitting μ_{obs} was $0.45\mu_B$ (μ_B is the Bohr magneton) for $LaCuO_{2.64}$, for instance, which is comparable to that of $0.68\mu_B$ previously reported for $LaCuO_{2.57}$.[19] However, all the measured values μ_{obs} are nearly half of the expected values μ_{cal}. Such small effective

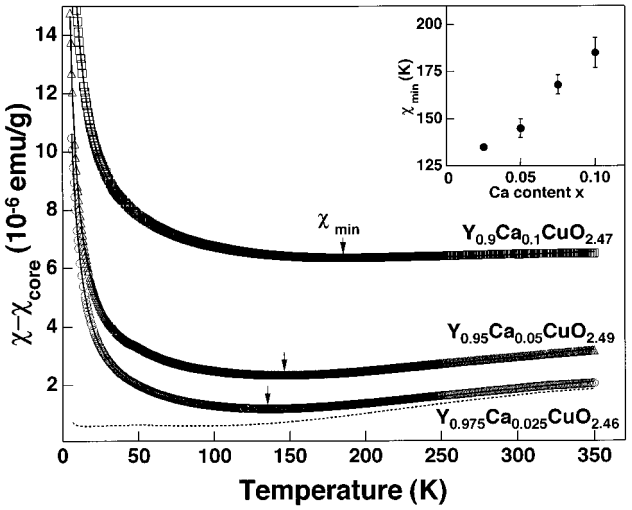

FIG. 10. Temperature dependence of the magnetic susceptibility (χ) for $(Y_{1-x}Ca_x)CuO_{2+\delta}$ samples after post-annealing in O_2 gas. The core diamagnetism $\chi_{\rm core}$ had been subtracted. For each sample, χ minimum ($\chi_{\rm min}$) is observed at temperatures marked with arrow. Solid line represents fitted curve based on the Troyer's equation [Eq. (4), see text]. After subtraction the Curie term, χ vs T curve is replotted especially for the sample with $\mathbf{x}=0.025$. Inset: the observed $\chi_{\rm min}$ with respect to Ca content, **x**.

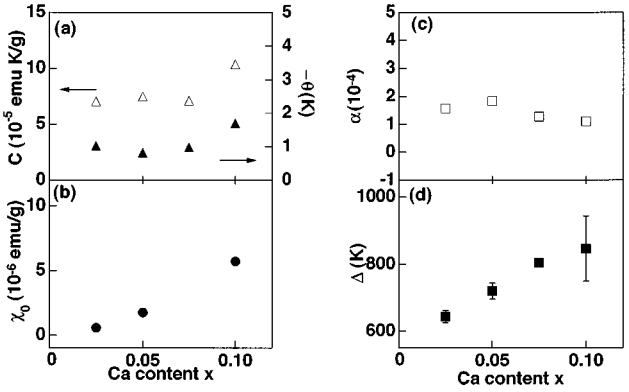

FIG. 11. Fitted parameters **C**, θ, χ_0, α, and Δ in Eq. (4) as a function of Ca content **x**.

magnetic moments may be a common feature for spin-frustrated systems.[27] As previously mentioned, some anomalies in the ρ vs T curve were observed for a couple of samples. According to Fig. 9(b), it seems that each χ^{-1} vs T curve deviates from straight line (marked with arrow) at a temperature corresponding to that detected for the anomalies in the ρ vs T curve. Therefore, the anomalies in resistivity are suspected to be caused by a certain magnetic ordering, probably by an ordering of spins of the rare-earth ions.

The χ vs T curves after subtracting the core diamagnetism $\chi_{\rm core}$ term are shown in Fig. 10 for oxidized $(Y,Ca)CuO_{2+\delta}$ samples. The $\chi_{\rm core}$ values were quoted from the literature; Y^{3+}:−24; Ca^{2+}:−13.3; Cu^{2+}:−13; O^{2-}:−12.6 (all in unit of 10^{-6} emu/mol).[26] Apparently, all the χ vs T curves exhibit a peculiar behavior. That is, for each sample, χ decreases gradually with decreasing temperature and shows a broad minimum ($\chi_{\rm min}$) at temperatures around 150 K, and finally follows a Curie-like behavior below 100 K. Furthermore, the temperature at which showed $\chi_{\rm min}$ was found to depend on the Ca content **x**, as clearly seen from the data given in the inset of Fig. 10. In this regard, the minimum in χ had also been observed in a high-purity non-Ca doped $YCuO_{2.51}$ sample at temperatures around 100 K,[19] but not in our $YCuO_{2.58}$ sample containing a large amount of impurity phase such as 3*R*-type $YCuO_2$.

Since the unusual temperature dependence of χ might be due to the presence of a spin gap we tried to analyze the χ vs T curve in the framework of $s=1/2$ Heisenberg antiferromagnet. The following two possible origins are considered in terms of conjunctions consisting of copper and oxygen ions. One possibility is simple chains of copper ions which are coupled to form 90° Cu-O-Cu bonds as in Sr_2CuO_3.[10,11] In this case, the temperature dependence of the susceptibility may be given theoretically by a Bonner-Fisher-type model as recently demonstrated by Motoyama and co-workers.[11,28,29] The other possibility is ladder chains of copper ions which are coupled to yield linear Cu-O-Cu bonds, and each ladder is coupled to form nearly 90° Cu-O-Cu bonds as in $SrCu_2O_3$.[1] In this case, experimental results are usually analyzed by employing Troyer's equation.[30] For the ''oxidized'' $(Y,Ca)CuO_{2+\delta}$ phases, on the other hand, the conjunction structures of the Cu-O bonds are not clearly known for the lack of structural refinement data at present. However, the decrease in χ resembles the behavior reported for the ladder compounds, $Sr_{n-1}Cu_{n+1}O_{2n}$ ($n=3,7$) (Ref. 1) and $(La,Sr)CuO_{2.5}$,[6] rather than that of the chain material, Sr_2CuO_3.[10]

Assuming that the magnetic property of the $(Y,Ca)CuO_{2+\delta}$ phases is dominated by a two-leg ladderlike Cu-O conjunction, we may discuss the χ vs T curve employing a similar scenario proposed for the ladder compounds. In a two-leg Heisenberg ladder, $\chi(T)$ is empirically expressed by the following formula:[30]

$$\chi(T)=\chi_0+\frac{C}{(T-\theta)}+\alpha T^{-1/2}\exp\left(\frac{-\Delta}{T}\right), \qquad (4)$$

where χ_0 is a temperature-independent term, the second term is a Curie-Weiss contribution to be attributed to lattice imperfections or impurity phases as discussed previously, and the third term is the susceptibility of a two-chain $s=1/2$ Heisenberg antiferromagnetic ladder at temperatures $T\ll\Delta$ as proposed by Troyer *et al.*[30] with α and Δ being a constant and the magnitude of spin gap, respectively. Temperature-independent χ_0 may be given by

$$\chi_0=\chi_{\rm core}+\chi_{VV}+\chi_{\rm Pauli}+\chi_{\rm Landau}, \qquad (5)$$

where $\chi_{\rm VV}$ is the Van Vleck term, $\chi_{\rm Pauli}$ is the Pauli paramagnetic contribution and $\chi_{\rm Landau}$ is the diamagnetic orbital contribution from conduction electrons. For conventional metals, $\chi_{\rm Landau}$ is simplified as $\chi_{\rm Landau}\propto -1/3\chi_{\rm Pauli}$,[31] so that it may be negligible.

The fitted curves based on Eq. (4) are replotted in Fig. 10 (solid lines). The fitting parameters are summarized in Figs. 11(a)–11(d) in terms of the Ca content **x**. As observed in Fig. 11(a), the Curie component is small for each sample such

that only 3.6–5.2 % of the free Cu^{2+} spins are effective if $s=1/2$ and $g=2$. This fraction of the Cu^{2+} spins is one-order of magnitude higher than that reported for $SrCu_2O_3$ (Ref. 1) and Sr_2CuO_3,[10] and of the same order as that reported for $(Sr,Ca)_{14}Cu_{24}O_{41}$.[5] Previously, Kato, Shiota, and Koike[5] proposed that among the two Cu sites in $(Sr,Ca)_{14}Cu_{24}O_{41}$, i.e., 2D Cu_2O_3 plane site and 1D CuO_2 chain site, the Curie component was from the Cu^{2+} spins in the CuO_2 chain site. Since the site for excess oxygen atoms in $(Y,Ca)CuO_{2+\delta}$ is presently unidentified, it is difficult to conclude whether the small value for the Cu^{2+} spin in this compound is intrinsic or not. For the sake of further discussions, we assume that the Curie component is from isolated defects or a certain impurity phase. Note that the interaction energy between the magnetic moments is negligibly small because the magnitude of θ is approximately 1 K for each sample. The increase in χ_0 with doping [Fig. 11(b)] may be attributed to the evolution of an in-gap state as proposed for $(La,Sr)CuO_{2.5}$.[6] As seen in Fig. 11(d), the magnitude of Δ is large ($\geqslant 600$ K), and it increases monotonically with increasing Ca content **x**. In ladders, the magnitude of superexchange coupling J is generally given by $J\sim 2\Delta$ on the basis of theoretical results,[8,29] and the χ vs T curve should have a maximum at the temperature which corresponds to J. Contrary to this expectation, a broad maximum in the χ vs T curve at a temperature around 400 K was reported for a non-Ca-doped $YCuO_{2.51}$ sample, for which the magnetic susceptibility was measured up to 700 K.[19] Thus, the chances are that the magnitude of Δ obtained by curve fitting in the present work may be overestimated by a factor of 2. Such a discrepancy could be caused by following reasons: (i) the ambiguity in curve fitting using Eq. (4) for the lack of χ vs T data at temperatures higher than 350 K, and/or (ii) a frustrated coupling constant λ may be taken into account in J. An underestimation in the magnitude of Δ when Eq. (4) was employed was pointed out for the ladder compounds $(Sr,Ca)_{14}Cu_{24}O_{41}$.[4,5]

Subtracting the Curie term, the magnetic susceptibility decreases gradually with decreasing temperature down to ~ 100 K, and then gets leveled off at low temperatures as shown in Fig. 10 for the $x=0.025$ sample (dashed line). Apart from the residual value at low temperatures, the curvature of the corrected χ vs T curve is rather similar to that for two-leg ladders in $SrCu_2O_3$, but unlike that for three-leg ladders in $Sr_2Cu_3O_5$ which is spin gapless. Now we suppose that the constant residual susceptibility represents contributions from χ_{VV} and χ_{Pauli} [in Eq. (5)]. Since both χ_{VV} and χ_{Pauli} have not been estimated for $(Y,Ca)CuO_{2+\delta}$, we employ typical values reported for some other cuprates, i.e., $\chi_{VV}=6\times 10^{-5}$ (emu/mol) for $LaCuO_{2.5}$ (Ref. 6) and $\chi_{Pauli}=5.01\times 10^{-5}$ (emu/mol) for $La_{1.95}Sr_{0.05}CuO_4$.[32] The sum of these values gives a similar figure to that observed for the residual susceptibility in the case of $x=0.025$ [$\sim 11\times 10^{-5}$ (emu/mol)]. Thus, the unusual temperature dependence of χ measured for $(Y,Ca)CuO_{2+\delta}$ is likely to indicate the presence of an energy gap in the spin-excitation spectrum, i.e., a spin gap.

Finally, we raise the following three questions. (1) Does the two-leg ladderlike Cu-O conjunction really exist in $(Y,Ca)CuO_{2+\delta}$? Such a conjunction may not be necessary to produce the observed magnetic properties. The existence of a spin gap was recently demonstrated in a ''plaquette''-type CaV_4O_9 phase.[33] In this structure, a depleted square lattice exists, and four-spin plaquettes are connected with their neighbors. Typical examples of spin gap were given by Ueda *et al.*; and others[34–38] as follows: (i) the $s=1$ antiferromagnetic Heisenberg chain, (ii) the double chain $s=1/2$ model, (iii) the $s=1/2$ Heisenberg antiferromagnetism in a *kagomé* lattice, and (iv) the Kondo spin-liquid phase in the Kondo lattice model at half filling. In order to refine the crystal structure of the present $RCuO_{2+\delta}$ and $(Y,Ca)CuO_{2+\delta}$ phase, neutron-diffraction measurements are in progress. (2) Why was such a spin-gap-like bulk susceptibility observed only in the case of $R=Y$? The difference in the crystal structure is a possible answer. That is, after sample annealing, only $(Y,Ca)CuO_{2+\delta}$ kept the orthorhombic symmetry, while other $RCuO_{2+\delta}$ phases were of the hexagonal $2H$-polytype. (3) If $(Y,Ca)CuO_{2+\delta}$ is a new spin-gap phase, why does the magnitude of Δ become larger upon carrier doping? Generally speaking, the magnitude of Δ in high-T_c superconducting cuprates gradually goes down to a value corresponding to the optimized T_c, i.e., T_c^{max} as carrier-doping proceeds in the underdoped region.[39] On the contrary, a slight increase in the magnitude of Δ by carrier doping was observed for two-leg ladders in $(La,Sr)CuO_{2.5}$.[6] Thus, it is still unclear how the carrier doping affects the magnitude of Δ. Measurements of the magnetic susceptibility at high temperatures up to $\leqslant 700$ K are in progress to obtain more precise values of Δ than those reported in this paper.

IV. SUMMARY

By thermal oxidation $RCuO_2$ and Ca-doped $YCuO_2$ samples yielded delafossite-derived $RCuO_{2+\delta}$ phases for rare-earth elements, $R=Y$, La, Pr, Nd, Sm, and Eu. The crystallographic structures of those phases were found to be of the hexagonal $2H$ polytype for $R=La$, Pr, Nd, Sm, and Eu, and orthorhombic for $R=Y$. The oxygen content in each $RCuO_{2+\delta}$ sample was analyzed by two different chemical methods and was confirmed to be ~ 2.6 per f.u. For all the samples, electrical resistivity exhibited semiconducting behavior at temperatures below 325 K, the magnitude being independent of the spices of R. An unusual temperature dependence of the magnetic susceptibility (χ), that χ decreased with decreasing temperature was observed for the Ca-doped $YCuO_{2+\delta}$ samples, but not for samples with $R=Y$. This unusual magnetic behavior was discussed using the model proposed for two-leg Heisenberg ladders in the framework of the $s=1/2$ Heisenberg antiferromagnetism. The curve fitting using Troyer's equation yielded a large value for the spin gap, $\Delta\geqslant 600$ K, and Δ was found to increase quasilinearly with increasing Ca content, x in $(Y_{1-x}Ca_x)CuO_{2+\delta}$.

ACKNOWLEDGMENT

The authors are grateful to Professor K. Yamada of Tohoku University for his helpful discussions.

*Author to whom correspondence should be addressed. Electronic mail: kazu@rdc.tohoku-epco.co.jp, Fax: +81-22-278-2176

[1] M. Azuma, Z. Hiroi, M. Takano, K. Ishida, and Y. Kitaoka, Phys. Rev. Lett. **73**, 3463 (1994).
[2] Z. Hiroi and M. Takano, Nature (London) **377**, 41 (1995).
[3] H. Yamane, Y. Miyazaki, and H. Hirai, J. Ceram. Soc. Jpn. **98**, 105 (1990).
[4] M. Uehara, M. Ogawa, and J. Akimitsu, Physica C **255**, 193 (1995).
[5] M. Kato, K. Shiota, and Y. Koike, Physica C **258**, 284 (1996).
[6] Z. Hiroi, Solid State Chem. **123**, 223 (1996).
[7] S. A. Carter, B. Batlogg, R. J. Cava, J. J. Krajewski, W. F. Peck, Jr., and T. M. Rice, Phys. Rev. Lett. **77**, 1378 (1996).
[8] T. M. Rice, S. Gopalan, and M. Sigrist, Europhys. Lett. **23**, 445 (1993).
[9] M. Uehara, T. Nagata, J. Akimitsu, H. Takahashi, N. Môri, and K. Kinoshita, J. Phys. Soc. Jpn. **65**, 2764 (1996).
[10] T. Ami, M. K. Crawford, R. L. Harlow, Z. R. Wang, D. C. Johnston, H. Huang, and R. W. Erwin, Phys. Rev. B **51**, 5994 (1995).
[11] N. Motoyama, H. Eisaki, and S. Uchida, Phys. Rev. Lett. **76**, 3212 (1996).
[12] K. Yamada, J. Wada, S. Hosoya, Y. Endoh, S. Nogushi, S. Kawamata, and K. Okuda, Physica C **253**, 135 (1996).
[13] H. Haas and E. Z. Kordes, Kristallografiya **129**, 259 (1969).
[14] T. Ishiguro, N. Ishizawa, N. Mizutani, and M. Kato, J. Solid State Chem. **49**, 232 (1983).
[15] H. Takei, Solid State Phys. **31**, 137 (1996) (in Japanese).
[16] J. P. Doumerc, A. Ammar, A. Wichainchai, M. Pouchard, and P. Hagenmuller, J. Phys. Chem. Solids **48**, 37 (1987).
[17] J. B. Goodenough, G. Gutta, and A. Manthiram, Phys. Rev. B **43**, 10 170 (1991).
[18] K. Imai, M. Koike, H. Takei, H. Sawa, D. Shimoi, K. Nozawa, and M. Kinoshita, J. Phys. Soc. Jpn. **61**, 1819 (1992).
[19] R. J. Cava, H. W. Zandbergen, A. P. Ramirez, H. Takagi, C. T. Chen, J. J. Krajewski, W. F. Peck, Jr., J. V. Waszczak, G. Meigs, R. S. Roth, and L. F. Schneemeyer, J. Solid State Chem. **104**, 437 (1993).
[20] K. Isawa, Y. Yaegashi, M. Komatsu, M. Nagano, and Y. Wakiya, *Advances in Superconductivity VIII* (Springer-Verlag, Tokyo, 1996), pp. 379–382.
[21] M. Karppinen, A. Fukuoka, L. Niinistö, and H. Yamauchi, Supercond. Sci. Technol. **9**, 121 (1996).
[22] R. D. Shannon, Acta Crystallogr. Sec. A **32**, 751 (1976).
[23] Pattern 39-0244, Powder Diffraction File of the Joint Committee on Powder Diffraction Data (International Center for Diffraction Data, Newtown Square, PA, 1995).
[24] D. B. Rogers, R. D. Shannon, C. T. Prewitt, and J. L. Gillson, Inorg. Chem. **10**, 723 (1971).
[25] J. B. Goodenough, in *Progress in Solid State Chemistry*, edited by H. Reiss (Pergamon, Oxford, 1971), Vol. 5, pp. 145–399.
[26] J. H. Van Vleck, *The Theory of Electric and Magnetic Susceptibilities* (Clarendon, Oxford, 1932).
[27] A. P. Ramirez, J. Appl. Phys. **70**, 5952 (1991).
[28] J. C. Bonner and M. E. Fisher, Phys. Rev. **135**, A640 (1964).
[29] S. Eggert, I. Affleck, and M. Takahashi, Phys. Rev. Lett. **73**, 332 (1994).
[30] M. Troyer, H. Tsunetsugu, and D. Würtz, Phys. Rev. B **50**, 13 515 (1994).
[31] A. H. Wilson, *The Theory of Metals* (Cambridge University, Cambridge, 1965), p. 155.
[32] D. C. Johnston, Phys. Rev. Lett. **62**, 957 (1989).
[33] S. Taniguchi, T. Nishikawa, Y. Yasui, Y. Kobayashi, M. Sato, T. Nishioka, M. Kontani, and K. Sano, J. Phys. Soc. Jpn. **64**, 2758 (1995).
[34] K. Ueda, H. Kontani, M. Sigrist, and P. A. Lee, Phys. Rev. Lett. **76**, 1932 (1996).
[35] F. D. M. Haldane, Phys. Lett. **93A**, 464 (1983).
[36] S. P. Strong and A. J. Millis, Phys. Rev. Lett. **69**, 2419 (1992).
[37] C. Zeng and V. Elser, Phys. Rev. B **42**, 8436 (1990).
[38] H. Tsunetsugu, Y. Hatsugai, K. Ueda, and M. Sigrist, Phys. Rev. B **46**, 3157 (1992).
[39] T. Tanamoto, H. Kohno, and H. Fukuyama, J. Phys. Soc. Jpn. **63**, 2729 (1994), and references therein.